Available online at www.sciencedirect.com
SCIENCE DIRECT®
Chaos, Solitons and Fractals 23 (2005) 1809–1817
CHAOS SOLITONS & FRACTALS
www.elsevier.com/locate/chaos

Local Lyapunov exponents for dissipative continuous systems

Florian Grond *, Hans H. Diebner

Center for Art and Media, Institute for Basic Research, Lorenzstr. 19, D-76135 Karlsruhe, Germany

Accepted 1 July 2004

Abstract

We analyze a recently proposed algorithm for computing Lyapunov exponents focusing on its capability to calculate reliable local values for chaotic attractors. The averaging process of local contributions to the global measure becomes interpretable, i.e. they are related to the local topological structure in phase space. We compare the algorithm with the commonly used Wolf algorithm by means of analyzing correlations between coordinates of the chaotic attractor and local values of the Lyapunov exponents. The correlations for the new algorithm turn out to be significantly stronger than those for the Wolf algorithm. Since the usage of scalar measures to capture complex structures can be questioned we discuss these entities along with a more phenomenological description of scatter plots.

1. Introduction

Lyapunov characteristic exponents (LCEs) are frequently computed measures for the characterization of chaotic dynamics. In the numerically inevitable case of temporal discretization, Δt, the LCEs Λ_i can be defined as follows:

$$\Lambda_i = \lim_{N\to\infty} \lim_{\Delta t\to 0} \frac{1}{N\,\Delta t} \ln[S_i(M_N)], \tag{1}$$

with

$$M_N = \prod_{i=0}^{N} \mathrm{e}^{J(i\,\Delta t)\Delta t}.$$

Hereby $S_i(M_N)$ denotes for the singular values of the matrix M_N and J for the Jacobian. As described in detail in [1,2] the M_N cannot be split into manageable subproducts. Thus, approximations of local contributions to the global term $S_i(M_N)$ have to be made. This is usually accomplished by an accumulation process during an iterative evaluation and re-orthonormalization of the variational equation along the trajectory of a dynamical system. The way in which this local contributions are computed depends on the used algorithm. Note, that unlike the global LCEs, Λ_i, the local Lyapunov exponents, $\lambda_i(t)$, do not obey an invariance principle, which is of importance with respect to time series

* Corresponding author.
E-mail address: grond@zkm.de (F. Grond).

0960-0779/$ - see front matter © 2004 Elsevier Ltd. All rights reserved.
doi:10.1016/j.chaos.2004.07.020

analyses [3]. Nevertheless, as we will point out in the sequel, it is worthwhile to investigate them, at least when dealing with simulated models.

When performing simulations on a computer, one usually has the freedom for arbitrarily choosing the coordinate system. However, within the chosen frame, non-invariant measures gain importance since they can supply additional information about the system under investigation. An example of such a measure is the non-uniformity factor (NUF) as described in [4], for example. So far the discussion of the NUFs, which are the standard deviations of the LCEs, are restricted to discrete unimodal maps. Locally reliable LCEs, however, allow to extend the NUF analysis to continuous systems [2].

We proceed by comparing a new algorithm introduced in [2] with the well known algorithm derived by Alan Wolf [5]. They are compared with respect to which algorithm supplies meaningful information in a local sense about the investigated dynamical system. Our arguments rely on the analysis of correlations. Thereby, the structure seen in different plots of point sets are captured by computing fractal dimensions that can be used, with a grain of salt, as a quantification of what the eye is immediately able to see in the graphical structures.

2. Comparison of the algorithms

2.1. Recapitulation of the new algorithm

Before comparing the two algorithms we briefly repeat the mayor changes with respect to the Wolf algorithm introduced in [2]. The new algorithm was developed starting out from the well known algorithm by Alan Wolf presented in [5], that built on previous work published in [6] and [7] (an early comprehensive description of different methods can be found in [8]). The reliability of the global measures derived by the Wolf algorithm can be confirmed. We observed, however, that the local contributions have to be considered with care.

To be more specific: all local values that contribute to the global positive or zero exponents represent arbitrary directions on the unstable manifold. Their arbitrariness can best be explained by considering the behavior of the zero exponent. As shown by Haken (for a proof cf. [1]) this exponent should represent the stretching and contraction along the tangential direction. However, the Lyapunov vector in phasespace that is associated to the accumulation of the zero exponent is anything but oriented in tangential direction when computed by the Wolf algorithm. The accuracy of Wolf's algorithm is usually founded in the self-orientation of the first Lyapunov vector towards the most unstable manifold. This most unstable direction coincides with the attractor but fluctuates in an unpredictable manner in the course of time. The new algorithm overcomes this problem by fixing the tangential direction as the first Lyapunov vector which corresponds to the zero exponent.

The development of the new algorithm was mainly based on the inspection of the visualized simulation containing topological information yielded by the variational equation. Although visual representations are still a contentious issue in branches of science that typically use formal mathematical approaches as a medium to express concepts, they are increasingly used as a potential source of knowledge, especially in complex systems research. Since we use in our research also visual-based methods the following investigation has been stimulated by an image shown in [9]. In this respect, it is also noteworthy that in the original publication of the Wolf algorithm an image was used to illustrate the performance of the algorithm. Obviously, the presented image did not cause changes in the design of the algorithm although, in our opinion, the image indicated insufficiencies that are now resolved with the new algorithm.

2.2. Analysis based on scatter plots

According to our previous considerations we will discuss the role of scatter diagrams away from ordinary applications in statistics which has been stimulated by a brief statement based on such a scatter plot given by Hoover [9]. He shows a plot of the local Lyapunov exponents $\lambda_1(t)$ versus the x-component of the chaotic Lorenz attractor. From this image he learns a certain relationship between the global invariant value and its local contributions [9, right part of Fig. 7.1 on p. 170]:

"The smooth time dependence contrasts with their highly-singular spatial dependence."

(The described image corresponds to Fig. 2b shown and discussed.) Given the image on which Hoover's statement is based we agree with him. The same image produced with the improved algorithm leads to a different situation (Fig. 2a). The new scatter plot seems to contain more coherent structure. Basically, we adopt Hoover's line of thought to use plots for inferences. Additionally to the obvious structure, we apply the fractal dimension to capture the complexity

quantitatively. This suggestion results from the fact that chaotic attractors are objects that hardly can be explained by linear statistical tools. This certainly holds for the relations of local properties on the attractor, too. Therefore we use the generalized dimension or Renyi spectrum to characterize the structure in the cloud of points in the resulting plots. The Renyi spectrum for a set of points is defined as

$$D_q = \lim_{\epsilon \to 0} \frac{1}{q-1} \frac{\ln C_q(\epsilon)}{\ln \epsilon}, \tag{2}$$

where

$$C_q(\epsilon) = \int_x x p(x)_\epsilon^{q-1} d\mu(x) = \left\langle p_\epsilon^{q-1} \right\rangle_\mu.$$

Confer [3] for a detailed introduction to the Renyi spectrum.

We have collected data to construct the three two-dimensional point sets $x(t)$ versus $\lambda_1(t)$, $y(t)$ versus $\lambda_1(t)$, $z(t)$ versus $\lambda_1(t)$ both for the Rossler and for the Lorenz attractor, respectively, as well as three-dimensional point sets from the local exponents $\lambda_1(t)$, $\lambda_2(t)$ and $\lambda_3(t)$. With minor exceptions, in the Renyi spectra calculated from these point sets the values for the new algorithm are lower then the corresponding values for the Wolf algorithm. A detailed description of the plots along with the aforementioned deviations is given below.

The result indicates that the difference between the two methods apparently found in the structure of the scatter plots can be confirmed by means of the quantitative measure supplied by their Renyi spectra.

2.3. Some specifications

Two well-known chaotic systems, the Rossler attractor

$$\begin{aligned} \dot{x} &= -(y+z), \\ \dot{y} &= x + ay, \\ \dot{z} &= b + xz - cz \end{aligned} \tag{3}$$

and the Lorenz attractor

$$\begin{aligned} \dot{x} &= \sigma(y-x), \\ \dot{y} &= \rho x - zx - y, \\ \dot{z} &= -bz + xy, \end{aligned} \tag{4}$$

have been used to investigate the algorithms. The parameters of the Rossler system have been chosen as: $a = 0.2$, $b = 0.2$, $c = 5.7$. The system was integrated with the Runge–Kutta method of fourth-order with a fixed step size $\Delta t = 0.003$. We skipped the transient by discarding 3000 steps. Every 3000th step was recorded in order to yield a point set that covers the whole attractor and omits autocorrelations which may lead to invalid dimension estimates. A total of 260,000 points has been recorded. A number of 170,000 reference points for the Renyi spectrum has been chosen.

The parameters for the Lorenz system are: $\sigma = 10$, $\rho = 25$, and $b = 8/3$. The integration method was as above with a step size of $\Delta t = 0.005$. The amount of 3000 steps were discarded to skip the transient. Every 500th step was recorded. 169,999 points were recorded and 160,000 reference points were used for the calculation of the Renyi spectrum.

The calculation of the spectra and the plots have been produced using the OPEN-TS tool for MatLab based on algorithms described in [10].

2.4. Description of plots

In Fig. 1 one can see the scatter-plots for the Rossler attractor. The left column of plots Fig. 1a, c and e, are the results for the new algorithm, whereas the column on the right-hand side, Fig. 1b, d and f, shows the results for the Wolf algorithm. Both plots 1a and 1b have the x-coordinate of the Rossler attractor as abscissa. Analogously, plots 1c and 1d have the y-coordinate of the Rossler attractor as abscissa and plots 1e and 1f the z-coordinate. The ordinate of all cases is the value of the positive local Lyapunov exponent $\lambda_1(t)$. The series of corresponding plots for the Lorenz attractor is depicted in Fig. 2.

Fig. 3 shows the pairwise Renyi spectra corresponding to the plots of Figs. 1 and 2. The dashed line is the spectrum for the Wolf algorithm and the full line for the new one. Specifically, parts Rossler a, Rossler b and Rossler c denote for the pairs of spectra that correspond to the pairs of point sets (1a, 1b), (1c, 1d), (1e, 1f), respectively, and analogously for the Lorenz cases, where Lorenz a, Lorenz b and Lorenz c correspond to the point sets (2a, 2b), (2c, 2d), (2e, 2f).

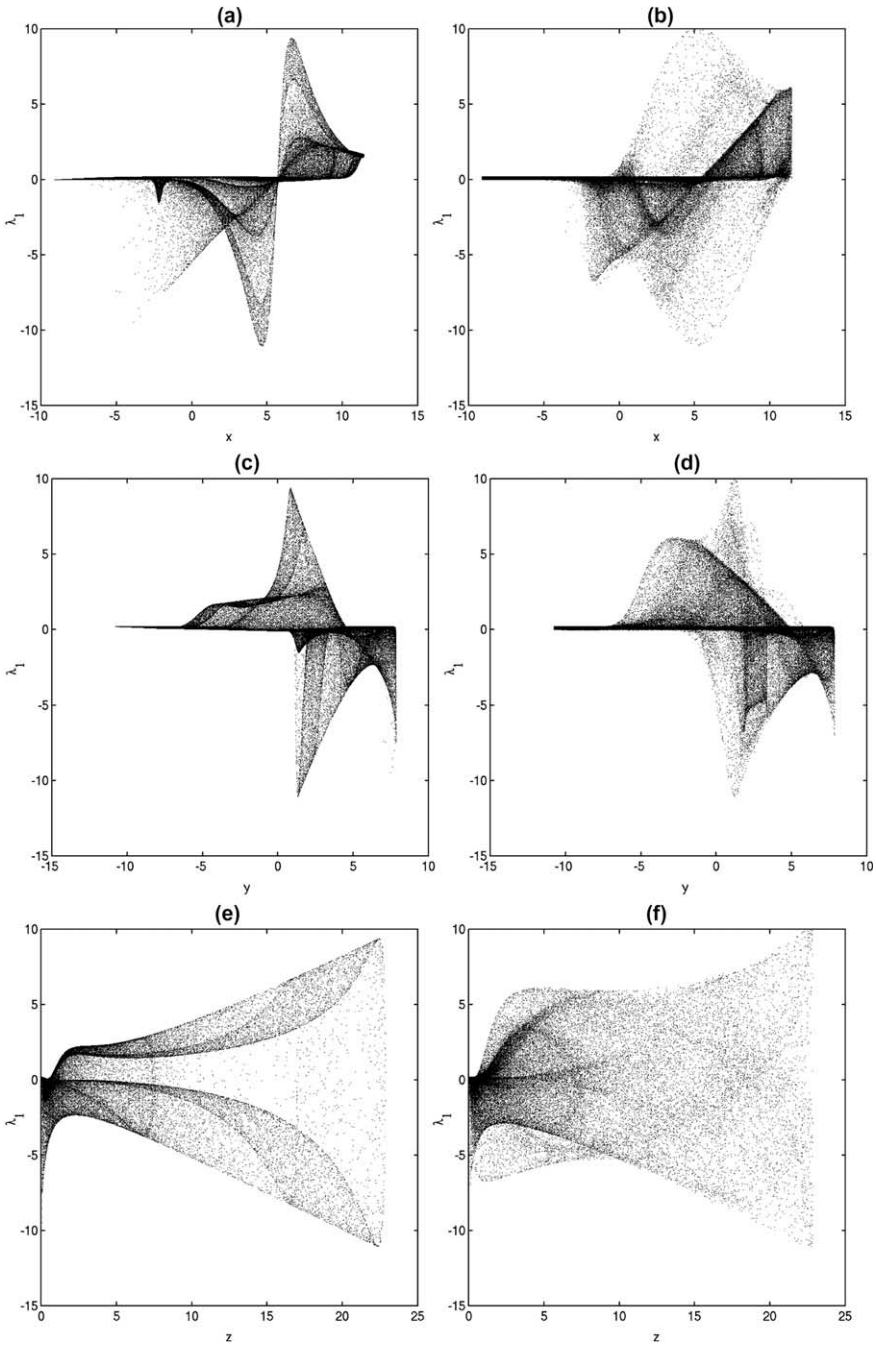

Fig. 1. Plots of the x-, y-, and z-coordinates of the Rossler attractor against the local Lyapunov exponent λ_1. The left column (a, c, and e) shows the results for the new algorithm, the right column (b, d, and f) for the Wolf algorithm.

Figs. 4 and 5 show scatter plots of all three local exponents $\lambda_1(t)$, $\lambda_2(t)$, $\lambda_3(t)$ that have been computed for the Rossler and the Lorenz attractors. Again, the two parts on the left-hand side show the results for the new algorithm and those corresponding to the Wolf algorithm on the right.

Fig. 6 shows the Renyi spectra computed from the point clouds of Figs. 4 and 5. The dashed lines denote for the Wolf algorithm, as before. Fig. 6a corresponds to Fig. 4 and Fig. 6b to Fig. 5.

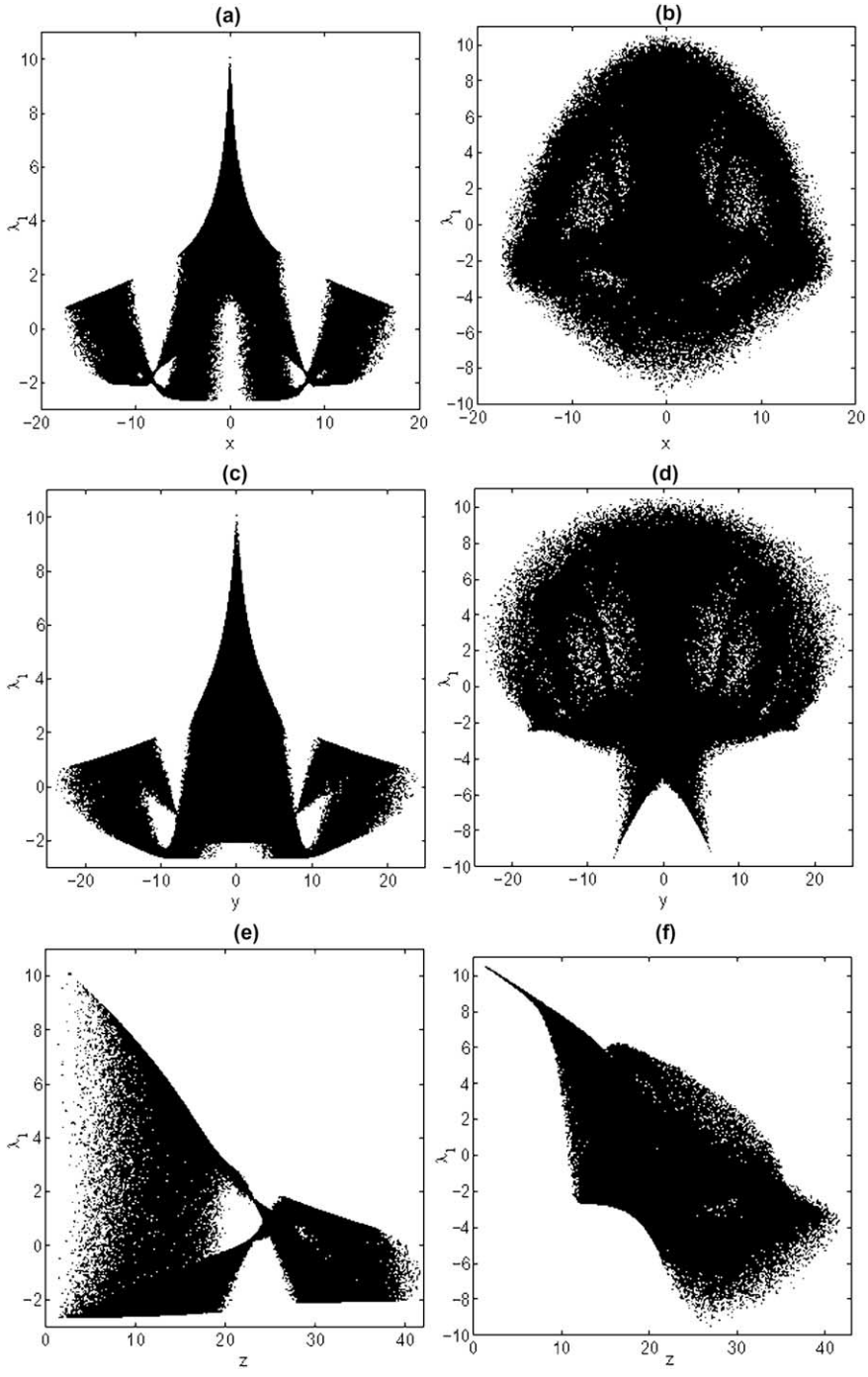

Fig. 2. Plots of the x-, y-, and z-coordinates of the Lorenz attractor against λ_1. As in Fig. 1, the left column (a, c, e) shows the results for the new algorithm, the right column (b, d, f) for the Wolf algorithm.

Obviously, the structures in all the point clouds produced with the new algorithm are much more coherent as those computed with the Wolf algorithm. In the Lorenz case depicted in Fig. 2, the λ_1–$x(t)$- and λ_1–$y(t)$-plots (Fig. 2a–d) show a symmetrical structure for both algorithms which is obviously related to the symmetry of the Lorenz system.

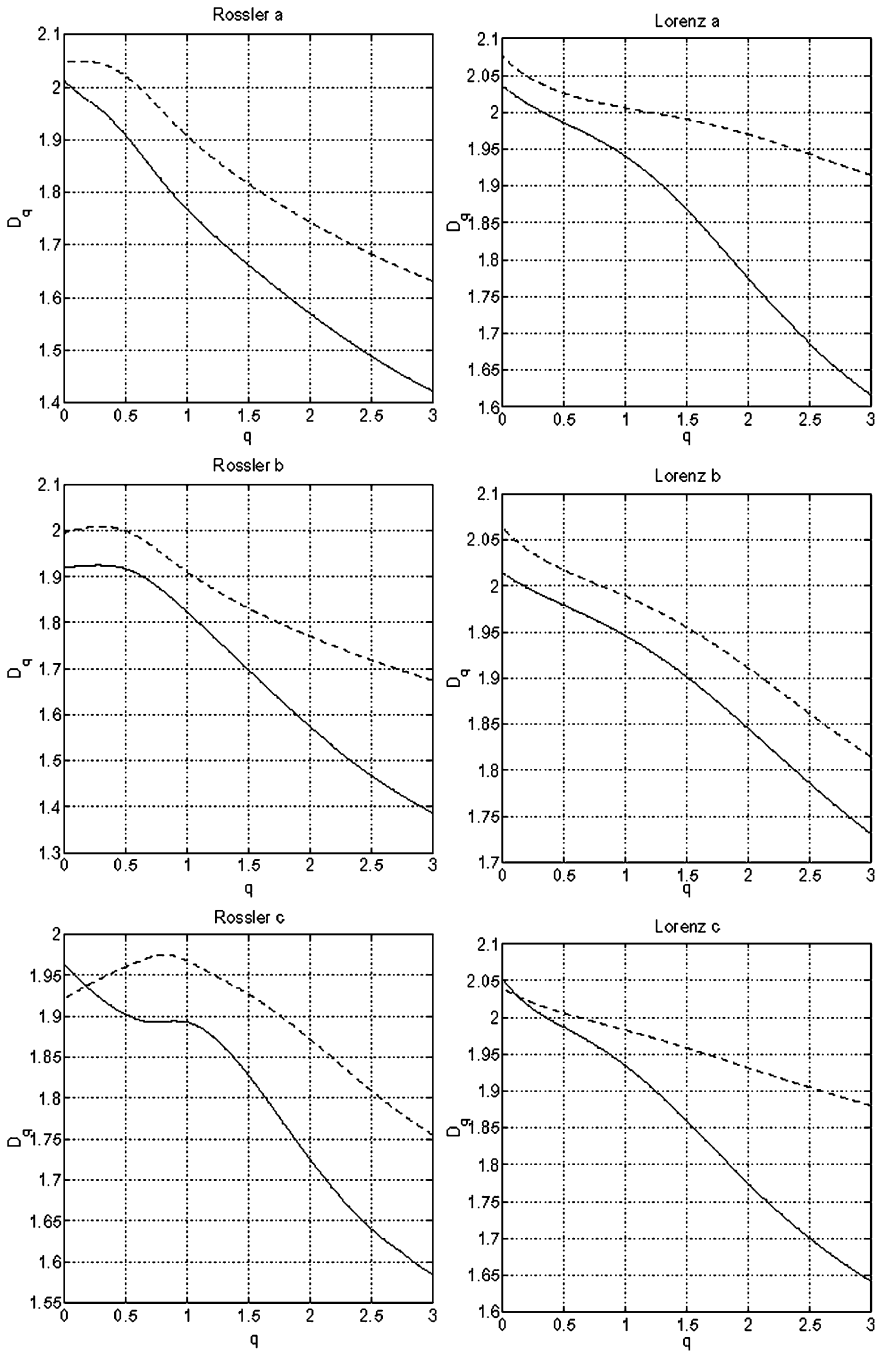

Fig. 3. Plots of the Renyi spectra computed from the point sets of Figs. 1 and 2. The left column shows the results for the Rossler attractor, the right column for the Lorenz attractor. The curve corresponding to the Wolf algorithm is shown as the dashed line. The full line belongs to the new variant.

Thus, a validation of the algorithm cannot be gained purely from this symmetry considerations. We proceed by estimating the fractal dimension and postpone a more visual-based discussion to the final part of the paper.

As already mentioned, one can see in the Renyi spectra that the Wolf algorithm produces larger values over the whole or at least a large part of the curves. Exceptions, where the curve corresponding to the Wolf algorithm lies below

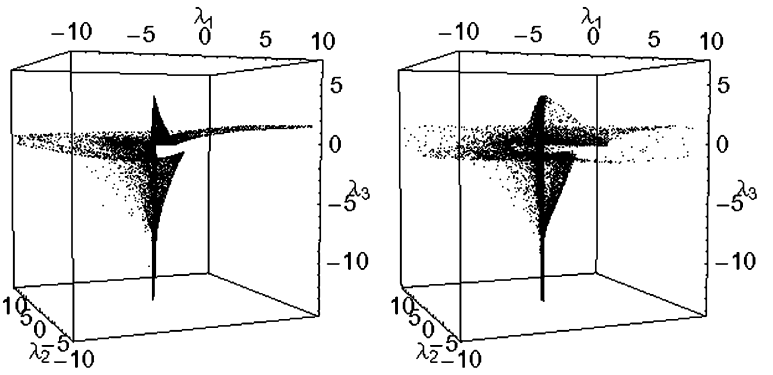

Fig. 4. Scatter plots of λ_1 vs. λ_2 vs. λ_3 for the Rossler attractor. The left part belongs to the new algorithm and the right one to the Wolf algorithm.

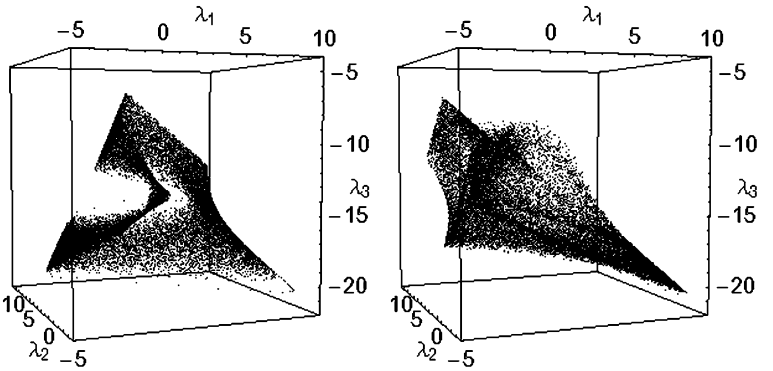

Fig. 5. Scatter plots of λ_1 vs. λ_2 vs. λ_3 for the Lorenz attractor. The left part belongs to the new algorithm and the right one to the Wolf algorithm.

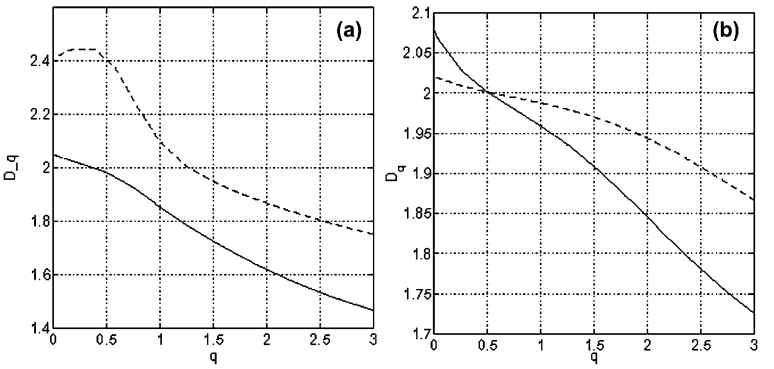

Fig. 6. Renyi spectra from the point sets in Figs. 4 (corresponding to (a)) and 5 (corresponding to (b)). The dashed line corresponds to the Wolf algorithm, the full line to the new one.

the curve belonging to the new one, can be observed for small values of q in three cases (Figs. 3 Rossler c, Lorenz c, and 6b). In general, the calculation of the fractal dimension with $q < 1$ is less robust (which is between the information dimension and the capacity dimension), as discussed in [3]. Systematic errors have to be taken into account in those cases. There are some cases where the dashed line (corresponding to Wolf's algorithm) increases as a function of q (Figs. 3 Rossler b, Rossler c, and 6a) which indicate systematic errors. In addition, the values of D_0 in some cases of Fig. 3 are

slightly greater than the maximum allowed value of 2 which is a further sign to take the values of D_q for $q < 1$ with a grain of salt.

On the other hand, for the new algorithm the function is everywhere decreasing with q in all plots. In the spectra from Fig. 6a and b, the lines intersect with the ordinate, i.e. for $q = 0$, at about $D_0 = 2$. This value is comparable to the capacity dimension of chaotic attractors of dissipative systems in three dimensions. Apart from the fact that in Fig. 6a the dashed line is not a decreasing function in q, one observes $D_0 \simeq 2.4$, a value that does not correspond to the fractal dimension of the Rossler attractor. Our speculation that the fractal dimension of the "Lyapunov space" is related to the corresponding dimension of the attractor in phase space remains to be proven.

The $\lambda_1(t)$–$z(t)$- as well as the $\lambda_1(t)$–$\lambda_2(t)$–$\lambda_3(t)$-plots of the Lorenz case (Fig. 2f and right part of Fig. 5) show that the spatial structure is partially destroyed and compactified by the Wolf algorithm. This may explain the behavior of D_q in Fig. 3 Lorenz c and Fig. 6b for small values of q.

3. Discussion

We have supplied additional support for the local reliability of the new algorithm to calculate Lyapunov exponents introduced in [2]. The arguments have mainly been based on the comparison of different plots of point sets. These scatter plots show correlations between the local Lyapunov exponents with respect to each other as well as correlations to the state variables of the Lorenz and the Rossler system, respectively. In addition to the obvious differences we found that the structures of the point sets are also different with respect to their fractal dimensions. We want the fractal dimension to be understood as a proposal to quantify correlations where linear measures fail. This is in fact one of the basic ideas of the correlation dimension D_2.

We are well aware, that our analysis so far lacks mathematical rigor. However, in the case of non-linear phenomena where closed solutions are often not available, the use of computer simulations and visualizations are not only helpful but inevitable. The use of images is a double-edged sword in such a situation, where they do not serve merely as illustrations. They become more than a didactical tool but rather a source of knowledge and make the scientists create hypotheses.

In the case in hand the images potentially provoke more questions than can be answered by a scalar complexity measure, where the latter is in a sense an antinomy, anyway. The reduction of complexity may be carried to far in this case. On the other hand, we have been stimulated by the comparison of the global correlation measures produced by the two algorithms to re-think the observed structures. For example, we observed a striking similarity in the fractal dimension of the attractor and the corresponding "Lyapunov space". This suggests a deeper relation like those known in dual spaces. The Rossler case, for example, shows a relation between the phase space and the Lyapunov space insofar as the capacity dimension $D_0 \simeq 2.05$ is approximately of the same value as the corresponding dimension of the attractor [11]. Note, that the Wolf algorithm produced a value of $D_0 \simeq 2.4$. For the Lorenz attractor the difference of the two algorithms is stronger reflected in the structures of the point clouds. Beyond the symmetry corresponding to the two "wings" of the Lorenz attractor in Fig. 2a–d the synchronous time behavior of x- and y-variables are stronger reflected in Fig. 2a and c that belong to the new algorithm. Further inferences and deductions are left to the reader with the recommendation to bear in mind that images often reveal as much as they cover. We hope to have brought forward convincing arguments to rethink the usage of Lyapunov algorithms.

Acknowledgments

We are grateful for discussions with Otto Rössler, Anton Huber and Inge Hinterwaldner. Special thanks go to Peter Weibel for his support and to Sebastian Fischer for discussions and his help in programming.

References

[1] Parker TS, Chua LO. Practical numerical algorithms for chaotic systems. New York: Springer Verlag; 1989.
[2] Grond F, Diebner HH, Sahle S, Mathias A, Fischer S, Rossler OE. A robust, locally interpretable algorithm for Lyapunov exponents. Chaos, Solitons & Fractals 2003;16:841–52.
[3] Kantz H, Schreiber T. Nonlinear time series analysis. Nonlinear science series. Cambridge: Cambridge University Press; 2002.
[4] Leven RW, Koch BP, Pompe B. Chaos in dissipativen Systemen. Berlin: Akademie Verlag; 1994.
[5] Wolf A, Swift JB, Swinney H, Vastano JA. Determinig Lyapunov exponents from a time series. Physica D 1985;16:285–317.

[6] Benettin G, Galgani L, Giorgilli A, Strelcyn J-M. Theorie ergodique. Compt Rond Acad Sci, Ser 1978;A:431–3.
[7] Shimada I, Nagashima T. A numerical approach to ergodic problems of dissipative dynamical systems. Progress Theoret Phys 1979;61:1605–16.
[8] Eckmann J-P, Ruelle D. Ergodic theory of chaos and strange attractors. Rev Mod Phys 1985;57:617.
[9] Hoover WG. Time reversibility, computer simulations, and chaos. Singapore: World Scientific; 2001.
[10] Parlitz U. Available from: http://www.physik3.gwdg.de/~ulli/reviews.html.
[11] Argyris J, Faust G, Haase M. Die Erfoschung des Chaos. Braunschweig: Vieweg Verlag; 1995.